Atmospheric
Measurement
Techniques
Discussions

Open Access

EGU

# An optical particle size spectrometer for aircraft-borne measurements in IAGOS-CARIBIC

M. Hermann[1], A. Weigelt[1,2,a], D. Assmann[1], S. Pfeifer[1], T. Müller[1], T. Conrath[1], J. Voigtländer[1], J. Heintzenberg[1], A. Wiedensohler[1], B. G. Martinsson[3], T. Deshler[4], C. A. M. Brenninkmeijer[5], and A. Zahn[6]

[1]Leibniz Institute for Tropospheric Research, Permoserstr. 15, 04318 Leipzig, Germany
[2]Helmholtz-Zentrum Geesthacht, Environmental Chemistry Department, Max-Planck-Straße 1, 21502, Geesthacht, Germany
[3]Lund University, Division of Nuclear Physics, Professorsgatan 1, 22363 Lund, Sweden
[4]University of Wyoming, Department of Atmospheric Science, 1000 E. University Avenue Laramie, WY 82071, USA
[5]Max Planck Institute for Chemistry, Air Chemistry Division, Hahn-Meitner-Weg 1, 55128 Mainz, Germany
[6]Karlsruhe Institute of Technology, Institute for Meteorology and Climate Research, Hermann-von-Helmholtz-Platz 1, 76344 Eggenstein-Leopoldshafen, Germany
[a]now at: Federal Maritime and Hydrographic Agency, Wuestland 2, 22589 Hamburg, Germany

11597

Discussion Paper | Discussion Paper | Discussion Paper | Discussion Paper |

Discussion Paper | Discussion Paper | Discussion Paper | Discussion Paper |

**Abstract**

The particle number size distribution is an important parameter to characterize the atmospheric aerosol and its influence on the Earth's climate. Here we describe a new Optical Particle Size Spectrometer (OPSS) for measurements of the accumulation mode particle number size distribution in the tropopause region onboard a passenger aircraft (IAGOS-CARIBIC observatory (In-service Aircraft for a Global Observing System – Civil Aircraft for Regular Investigation of the Atmosphere Based on an Instrument Container)). A modified "KS93 particle sensor" from RION Co., Ltd. together with a new airflow system and a dedicated data acquisition system are the key components of the CARIBIC OPSS. The instrument records individual particle pulses in the particle size range 130–1110 nm diameter (for a particle refractive index of 1.47-i0.006 for an upper tropospheric (UT) aerosol particle) and thus allows the post-flight choice of the time resolution and the size distribution bin width. The CARIBIC OPSS has a 50 % particle detection diameter of 152 nm and a maximum asymptotic counting efficiency of 98 %. The ~~instruments~~ measurement performance shows no pressure dependency and no coincidence for free tropospheric conditions. The size response function of the CARIBIC OPSS was obtained by a polystyrene latex calibration in combination with model calculations. Particle number size distributions measured with the new OPSS in the lowermost stratosphere agreed within a factor of two in concentration with balloon-borne measurements over western North America. Since June 2010 the CARIBIC OPSS is deployed once per month in the IAGOS-CARIBIC observatory.

## 1 Introduction

The particle number size distribution is essential to describe the physical properties of the atmospheric aerosol and its influence on climate (Charlson et al., 1992; Mann et al., 2014). In particular in the accumulation mode (particles with diameters of 0.1–1.0 μm) this information is of interest, because this mode dominates in most cases the

11599

particle surface area concentration and thus the radiative properties of the atmospheric aerosol (Seinfeld and Pandis, 1998). Moreover the accumulation mode dominates the total particle mass concentration in air masses without coarse mode particles (particle diameter larger than 1.0 μm), for instance in the upper troposphere and lowermost stratosphere (UT/LMS).

Particle number size distribution can be sensed either remotely or in situ. Remote sensing methods have the advantages of providing vertical information (e.g., by lidars) or near-global coverage (by satellite instruments). However, particle number size distributions derived from remote sensing methods bear large uncertainties. Furthermore, in the free troposphere, where the aerosol mass load usually is low, some instruments have problems to identify aerosol signals because of their detection limits (Winker et al., 2013). In situ particle number size distribution measurements give the most detailed information and can be used to validate remote sensing results. Commonly used are Mobility Particle Size Spectrometers (MPSS, Wiedensohler et al., 2012) and Optical Particle Size Spectrometers (OPSS, Gebhardt, 2001). An OPSS, as discussed in this paper, measures the light scattered by individual particles to derive their number and diameters. The relationship between particle diameter and scattered light~~s~~ is mostly established in the laboratory usually by calibration with polystyrene latex (PSL) particles. For aircraft-borne measurements, OPSS are preferably used (e.g., de Reus et al., 2000, 2001; Krejci et al., 2003; Schröder et al., 2002; Young et al., 2007; Zaizen et al., 2004) because they can measure relatively fast and do not have problems with the aviation permission (in contrast to MPSS systems with radioactive chargers). However, calibration of OPSS, as described here, is always an issue (e.g., Rosenberg et al., 2012; Cai et al., 2013) because of the effects of particle refractive index and shape.

Aside from the long-term balloon-borne measurement series at Laramie, Wyoming (Deshler et al., 2003), there have been no regular in situ measurements of the accumulation mode particle number size distribution in the UT/LMS. In this study we present a new OPSS applied for regular measurements of the UT/LMS particle number size distribution onboard a passenger aircraft. Particle size distributions measured by this

11600

instrument were already used in previous studies (Rauthe-Schöch et al., 2012; Martinsson et al., 2014; Andersson et al., 2015). Here we present details of the measurement system (Sect. 2). The new OPSS was characterized in the laboratory with respect to particle pulse signals, pressure dependency, particle sizing, particle counting efficiency, and particle coincidence (Sect. 3). A post-flight data processing routine was developed and measurement uncertainties were assessed (Sect. 4). Since June 2010 the OPSS is operated on two to four intercontinental flights per month as part of the scientific payload onboard a Lufthansa Airbus A340-600 within the CARIBIC part (Civil Aircraft for Regular Investigation of the Atmosphere Based on an Instrument Container, www.caribic-atmospheric.com, last access: 1 July 2015, and Brenninkmeijer et al., 2007) of the European Research Infrastructure IAGOS (In-service Aircraft for a Global Observing System, www.iagos.org, last access: 1 July 2015). Examples of two flights provide an impression on the UT/LMS aerosol data obtained (Sect. 5).

## 2 CARIBIC OPSS description

### 2.1 Original instrument: the RION particle sensor KS-93

Although the CARIBIC measurement container weighs 1.6 tons and is three meters wide, the large number of experiments onboard forces a focus on small and light equipment with low power consumption. Besides these constraints we required an instrument with a lower size detection limit below 200 nm equivalent optical particle diameter. These requirements are fulfilled by the "KS-93 particle sensor" (RION CO., Ltd., Japan, www.rion.co.jp/english/, last access: 1 July 2015), an instrument developed for semiconductor manufacturing applications, which had not been applied to airborne atmospheric research before. The KS-93 particle sensor (Fig. 1) is light (6.5 kg) and small (135 mm × 280 mm × 150 mm) and has a robust synthetic quartz optical cell, which makes it all well suited for airborne aerosol research. The KS-93 optics uses perpendicular polarized light from a diode laser with 830 nm wavelength and a light detec-

tion system at $90° ± 40°$ collecting angle. The manufacturer specifies particle number concentration measurements in five size channels between 0.1 and 2.0 µm optical particle diameter with 50 % counting efficiency. To cover the whole particle signal range of more than four orders of magnitude, the KS-93 uses three linear amplifiers. In order to increase the number of size channels by using a new data acquisition it was necessary to directly access the scattered light signals. Therefore RION modified one KS-93 for CARIBIC and installed three new SMB (miniature coaxial RF) connectors at the KS-93 rear plate, which allow direct access to the particle signals of the three amplifiers. The volume flow through the KS-93 can be varied between 0.05 and 0.3 L min$^{-1}$ and must be externally controlled.

### 2.2 CARIBIC OPSS

The modified KS-93 is mounted together with the flow control system and the new data acquisition in a 19″ EMC rack unit (Fig. 2, chassis: Knürr, Markt Schwaben, Germany). As the aerosol inlet and outlet of the KS-93 are glued to the quartz optical cell inside the KS-93 the instrument is somewhat sensitive to shocks and vibration. Therefore the modified KS-93 was mounted in a dedicated aluminum frame, which is fixed on the ground plate by three wire rope isolators (Enidine, Orchard Park, NY, USA). Because of this construction, all air tubing to the modified KS-93 (electro-conductive silicone tubing with 4.83 mm inner diameter, TSI, Shoreview MN, USA), as well as power and signal cables are flexibly connected. Besides the modified KS-93, the CARIBIC OPSS houses the data acquisition, the flow control system (e.g., mass flow controllers (Bronkhorst, Ruurlo, the Netherlands), and a small pump/compressor (KNF Neuberger, Freiburg Germany), sensors for temperature and pressure as well as electronic components (e.g., EMI filter, DC/DC converter). Access to the CARIBIC OPSS is provided via the front plate, where the power and communication connectors are located. In the rear plate, the CARIBIC OPSS has a Compact Flash (CF) data card slot, where the measurement data are stored and can be accessed. The sample air enters the CARIBIC OPSS through the front plate and leaves the instrument through the rear plate, where

a vacuum source must be applied. For CARIBIC this is a common diaphragm pump (Vacuubrand, Wertheim, Germany) in another rack unit, used for all CARIBIC aerosol instruments, including three Condensation Particle Counters (Hermann and Wiedensohler, 2001) and an aerosol impactor sampler (Nguyen et al., 2006).

To obtain the aeronautic certification for the aircraft, all materials must be non-flammable (e.g., Teflon-covered cables) and all fasteners to be secured against loosening. Moreover, the CARIBIC OPSS had to pass an Electro Magnetic Compatibility (EMC) test (RTCA DO-160E) ensuring that it does not interfere with the aircraft electronic systems.

A schematic of the CARIBIC OPSS sample and auxiliary airflow system is shown in Fig. 3. There are two basic operating states. In the stand-by mode (green arrows in Fig. 3), the two-way selector valve is switched in position 1 > 3 and the internal diaphragm pump blows about $3\,\mathrm{L\,min^{-1}}$ of filtered air into the tubing system. As both mass flow controllers (MFCs, Bronkhorst) are closed and the external vacuum pump is not switched on, the $3\,\mathrm{L\,min^{-1}}$ are pushed through the flow splitter and the sample air inlet out of the CARIBIC OPSS into the aerosol inlet system in the aircraft. This purging mechanism is in operation during aircraft takeoff and landing to prevent contamination of the sampling line and all aerosol instruments by polluted air in the vicinity of airports.

In measuring mode (blue arrows in Fig. 3) the two-way selector valve is switched in position 1 > 2 and the external vacuum pump is switched on. In this mode, particle-free sheath air is applied around the aerosol sampling air by adjusting MFC1 to $0.150\,\mathrm{L\,min^{-1}}$ and MFC2 to $0.134\,\mathrm{L\,min^{-1}}$ (see Sect. 3.2). Using the pressure and the temperature data from the sensors in the airflow, the MFCs are adjusted to a constant volume flow through the optics by a 1 Hz LabVIEW proportional-integral-derivative (PID) controller algorithm. This measure guarantees for each MFC a constant air volume flow with 1 % accuracy despite pressure changes during flight. MFC2 provides only 90 % of the air sucked through the optics to the vacuum (the sheath air). The residual sample airflow of $0.016\,\mathrm{L\,min^{-1}}$ is taken from the CARIBIC aerosol inlet, via a flow splitter and the sheath air device upstream the KS-93 optics. To reduce the

residence time of the sample air in the sampling line between the inlet at the aircraft fuselage and the aerosol instruments in the container and to minimize wall effects only the core flow is transported to the aerosol units using a first flow splitter (not shown). The particle-depleted air near the tubing wall ($\sim 4.2\,\mathrm{L\,min^{-1}}$, flow splitter excess air) is sucked to the vacuum. This excess airflow is controlled by a critical orifice. From the first flow splitter about $1\,\mathrm{L\,min^{-1}}$ of measurement air is sucked through a 1 m long 1/4″ tubing to the second flow splitter inside the CARIBIC OPSS. At the second flow splitter, which is located about 10 cm upstream of the sheath air insertion point, again only the less influenced core flow ($0.016\,\mathrm{L\,min^{-1}}$) is utilized for the particle measurement. The rest, the OPSS excess air, is sucked to the vacuum, again controlled by a critical orifice. The pressure of the external vacuum is monitored in another aerosol rack unit and remains always below 40 % of the operation pressure at the CARIBIC OPSS inlet, thus ensuring proper critical orifice operation.

## 2.3 Data acquisition and unit control

In the KS-93 particle sensor the scattered light from each particle is sensed by a photodiode and the respective particle signal is amplified in parallel by the three internal linear amplifiers. In the CARIBIC OPSS the output of these amplifiers is recorded with a real-time data acquisition system (PXI, National Instruments Germany, Munich, Germany) with 3 µs time resolution. As the pulse of a single particle has a duration of about 60 to 90 µs (see Fig. 5), each pulse is thus resolved with 20 to 30 data points. This data acquisition allows a free and individual choice of the averaging time and number of size channels at any time after a flight. For the current version of the CARIBIC OPSS data (V14) particle pulse height maxima are sorted into 10 channels and averaged over 180 s. Besides the particle signals, the data acquisition also records housekeeping data (operating pressure, measurement air and unit temperatures, and mass flows) with 10 Hz resolution. All routines are written in LabVIEW (National Instruments, Germany, Munich, Germany).

## 3   CARIBIC OPSS characterization

### 3.1   OPSS calibration set-up

For the calibration of the CARIBIC OPSS with respect to particle size and counting efficiency, measurements with different particle sizes were carried out (Fig. 4). The particle material (PSL or ammonium sulfate (AS)) was suspended in de-ionized water (1). After nebulizing this suspension in a TSI 3076 particle generator (nebulizer) (2), the aerosol was directed into a droplet trap (3). While large droplets were removed by impaction, the small ones followed the air stream into a glass bottle dilution unit (4). In this glass bottle the calibration air was mixed with dry particle-free air to reduce the total particle number concentration and to dry the droplets. By adjusting the dilution ratio the particle number concentration of the measurement air was set between 20 and 1000 cm$^{-3}$. To obtain really dry particles, the aerosol passed an additional silica-filled diffusion drier (5). When PSL calibration standards (Duke Scientific Corporation, Nanosphere Size Standards NIST Traceable Mean Diameter, Thermo Fisher Scientific Germany, Braunschweig, Germany) were used, the resulting particle number size distribution downstream the drier was quasi-monodisperse. However, some particles, much smaller than the specified PSL particle diameter were present due to the remaining impurity of the nebulized water ("water peaks"). Therefore the quasi-monodisperse PSL particles were charged inside a bipolar diffusion charger (Am$^{241}$) (6) and size-separated using a Differential Mobility Analyzer (DMA, Vienna type) (7). Downstream

11605

the DMA the monodisperse PSL aerosol was directed to the CARIBIC OPSS (8a). As reference instrument for the particle number concentration a Condensation Particle Counter (CPC, TSI Model 3010, 8b) was used, which has the same volume flow rate of 1 L min$^{-1}$ as the CARIBIC OPSS. Particle losses due to sedimentation, impaction, and diffusion were minimized by avoiding strong tube bends and keeping the tubing as short as possible. For the determination of the CARIBIC OPSS counting efficiency, particles with many different particle diameters were needed, hence, AS particles were generated in a similar way, as described for PSL above.

### 3.2   OPSS particle pulse signals

To cover a wide particle size range, the scattered light signal is amplified in the KS-93 by three individual linear amplifiers. The amplifier outputs are connected to the newly installed SMB connectors, called channels one to three (Ch1–3). The amplified particle pulses have roughly a Gaussian shape and amplitudes of 0 to 10 V (see Fig. 5). The signal of Ch1 is amplified most strongly to resolve the signals of particles smaller than about 234 nm diameter (with respect to an UT particle refractive index of 1.47-i0.006; see Sect. 3.4). Particles larger than about 234 nm and smaller than about 515 nm are resolved best with the second channel (Ch2). All larger aerosol particles are resolved only in the third channel (Ch3). The upper limit of Ch3 and therefore the upper limit for size resolved measurements of the OPSS is given by the saturation of the third amplifier (10 V signal) and was analyzed to be at about 1110 nm diameter for the current OPSS flow set-up. The OPSS counts also particles larger than 1110 nm, but as these particles yield a 10 V primary signal they are not size resolved but all registered at the same size. Figure 5 shows two examples for a typical signal of a 200 nm and a 900 nm diameter PSL particle with a complex refractive index of $m = 1.59$–0.0i. The 200 nm particles cause on average signal pulses with a duration of about 60 µs and a maximum pulse height of 6.6 V in Ch1 (Fig. 5a). The maximum of Ch2 and Ch3 is on average 0.22 and 0.05 V, respectively. For larger particles with a diameter of for instance 900 nm, the amplifiers of Ch1 and Ch2 are saturated and therefore the signal is truncated at 10 V

11606

(Fig. 5b). This particle size is resolved in Ch3 with a pulse width of about 90 μs and an average pulse height of 8.65 V.

For data analysis, the signals of the three channels are combined to one quantitative signal for each particle. Therefore the signals from Ch2 and Ch3 were multiplied with a factor of 30 and 125, respectively, leading to a combined signal in the range of 0 to 1250. The comparison of the three amplified signals (Fig. 5c and d) shows a good agreement, which gives confidence in the amplification factors for Ch2 and Ch3. As Ch1 is the most sensitive, the signal recording of all three channels is triggered by the intensity of Ch1. The trigger level was set to 0.35 V as for measurements of particle-free air and a trigger level of 0.30 V small noise signals were recorded. This trigger level determines the lower detection limit of the OPSS, which is calculated to be about 130 nm (UT aerosol; see Sect. 3.5).

First calibrations of the modified KS-93 showed the occurrence of spurious particle signals in the size spectrum. As example, Fig. 6a shows the output signal distribution for 350 nm PSL particles. The experimental set-up (Sect. 3.1) provides a narrow, i.e. monomodal aerosol particle number size distribution. Besides the main peak, the signal spectrum of the modified KS-93 contained also a significant number of counts, which had smaller signals, suggesting the existence of smaller particles. The additional small signals were only observed when measuring particle-loaded air. Hence the additional small signals were not caused by some kind of background noise. A potential reason for this signal intensity spread was thought to be the sampling flow geometry in the KS-93 optics. Particles passing the laser beam not in its center, but in the edge region with reduced illumination, might cause smaller particle signals. To focus the aerosol particles to the center of the laser beam, the measurement air was surrounded by particle-free sheath air in the new flow system of the CARIBIC OPSS. This sheath air is pushed through the side branch of a Swagelok tee mounted upstream the KS-93 inlet and nestled around a 1/16″ tubing for the sampling air located at the union center line. Using this set-up four sampling-to-sheath-air ratios in the range of 1 : 3 to 1 : 15 were tested. With increasing fraction of the sheath air, the number of spurious

signals decreased. However, considering that reducing the sampling air volume flow rate causes a reduction of the CARIBIC OPSS time resolution (because of sampling statistics), a sample-to-sheath-air ratio of 1 : 9 was chosen. Figure 6b shows again the distribution of the signal intensity for 350 nm PSL particles, this time with sheath air. Clearly, the number of artifact particle signals is reduced, but it did not totally vanish. Furthermore, the 350 nm particle peak becomes narrower and its maximum is shifted to slightly larger signal intensities, both as an effect of the focusing the particles into the region with the highest laser light intensity.

The distribution of particle signals shows an increasing fraction of spurious particles and an increasing apparent particle diameter of the spurious particles with increasing real particle diameter. Using approximate relations for this behavior and six UT/LMS particle number size distributions from the literature (de Reus et al., 2000, 2001; Krejci et al., 2003; Schröder et al., 2002; Young et al., 2007; Zaizen et al., 2004), the error caused by the spurious particle pulses to the real particle number size distribution was estimated. As the UT/LMS particle number size distribution shows a steep decrease by at least two orders of magnitude in the size range 0.1 to 1.0 μm (see e.g. Fig. 13), the error caused by the spurious particles is negligible for particles larger than 230 nm (smaller than 2 % increase in particle number concentration) and relatively small for particles below 230 nm (an increase of 2–10 %), compared to other uncertainties in the CARIBIC OPSS measurements (see Sect. 4.3).

We further investigated how to reduce this unsatisfactory feature of the CARIBIC OPSS. It turned out when looking at the particle inter-arrival times that not all inter-arrival times follow the expected exponential distribution, but some pulses show up at very short inter-arrival times. As an example, in Fig. 7 the inter-arrival times from a calibration run with 500 nm PSL particles and a number concentration of about 60 cm$^{-3}$ are displayed. About 93 % of the particle pulses in the first two bins to the left turned out to be spurious pulses, as they cause signals below 20 V, which is much lower than the 420 V for 500 nm PSL particles. Thus for UT/LMS measurements it is possible to suppress the concentration increase caused by artificial particle pulses to a negligible

level by applying an inter-arrival time filter of 0.0019 s to the measurement data, which was done for all CARIBIC flight data. However, in cases where the particle number size distribution does not fall off as steeply, like for measurements in the atmospheric boundary layer, the influence of the spurious signals cannot be neglected anymore. In this case also the inter-arrival time filter does not work properly because the particle number concentration is so high that artifact and real particle pulses are not well separated anymore in the inter-arrival time diagram. For the current set-up this is the case for particle number concentrations above about 200 cm$^{-3}$ in the accumulation mode. For such an application additional efforts would be needed to correct for this effect.

### 3.3 Pressure dependency of the OPSS particle signal

Onboard the CARIBIC aircraft, the CARIBIC OPSS experiences operating pressures in the range of 250 to 1100 hPa. The material of the optics (synthetic quartz cell) and the operating pressure of up to 5000 hPa specified by the manufacturer suggest no pressure dependency of the KS-93 signals. To verify this assumption the signal of 450 nm PSL particles was recorded at six pressures between 200 and 1000 hPa. For this purpose a pressure reducing valve and a pressure sensor were installed in the calibration set-up (Fig. 4) just upstream the CARIBIC OPSS. The resulting average pulse signals are displayed in Fig. 8. Although there seems to be a trend towards higher particle signals with decreasing operating pressure, this trend is only weak, with a maximum change less than 3 % in particle diameter. This uncertainty is much smaller than the uncertainty caused by the unknown refractive index of the measured atmospheric particles (15 %, see Sect. 4.3). Moreover, the experimental data almost exclusively agree within the experimental uncertainties (here defined as plus/minus one size channel (out of 230 in total) compared to the size channel with the peak maximum). Consequently there is no significant pressure dependency of the signals and thus final data are not corrected for pressure effects.

11609

### 3.4 OPSS particle sizing

To determine the relation between the particle pulse height maximum and the corresponding particle diameter, the CARIBIC OPSS response function had to be determined. For this purpose calibration measurements with PSL particles were carried out and the theoretical response function was calculated for perpendicular polarized light and spherical PSL particles (refractive index of 1.578-i0.0006). The calculation of the response function is based on exact optical Mie-calculation (Bohren and Huffman, 1983) in combination with a Levenberg-Marquardt algorithm for nonlinear multivariate fitting. The model considers the effects of laser polarization and spherical aperture or detection area. As free parameters the mean collecting angle, the collecting angle range, and the signal gain were used, whereas the refractive index, the polarization, and the laser wavelength were kept constant. The best fit to the PSL data points, shown in Fig. 9a, was achieved with mean collecting angle of 86.3°, a collecting angle range of ±34.8°, and a signal gain of 4016. The difference to the manufacturer values of 90° for the mean collecting angle and ±40° for the collecting angle range is caused by the non-ideal behavior of the optics, the changed aerosol flow through the KS-93, and the limitations of the theory underlying the fit algorithm. With the above geometry parameters, the measured data can be reproduced very well and hence they were used for all other response function calculations.

The use of perpendicular polarized light in the KS-93 has the advantage of reaching a lower detection limit diameter (Bohren and Huffman, 1983), but leads to a first Mie resonance (i.e. an ambiguity in the signal-to-particle-size relation) already just above 500 nm diameter (Fig. 9a). As the polarization of the KS93 cannot be easily changed, for spherical particles the choice of size channel borders for the KS93 is therefore somewhat limited.

In order to derive the CARIBIC OPSS response function for UT/LMS particles a refractive index for these particles has to be assumed. Based on literature values (e.g., GEISA spectroscopic data base at www.pole-ether.fr, last access: 1 July 2015) a uni-

11610

form refractive index of 1.47-i0.006 was chosen for the CARIBIC particle number size distributions (data set version 14). This value is derived assuming an internally mixed aerosol of 45 % sulfuric acid/water, 44 % ammonium sulfate, 10 % organics, and 1 % soot for a mid-latitude UT aerosol and using a volume-mixing rule for the refractive index. The choice of this refractive index is somewhat arbitrary, but not unrealistic, as the particle composition in the UT/LMS changes with altitude (Murphy et al., 2014). However, in order to have a uniform data set without discontinuities it was necessary to use only one refractive index. A sensitivity analysis on the influence of the refractive index on the derived particle size shows that the particle number size distribution would be shifted on average by 15 % in diameter towards larger diameters, if for instance the refractive index of sulfuric acid/water (1.43-i0.001) representative for a stratospheric aerosol would be used (see Sect. 4.3). With the PSL-fit-determined geometry parameters the CARIBIC OPSS response function for spherical particles and a UT/LMS refractive index of 1.47-i0.006 was calculated and is shown in Fig. 9b.

Unfortunately, the Mie resonance above 500 nm particle diameter also exists for the UT/LMS response function. Varying the refractive index in the range of 1.39 and 1.55 for the real and 0.002 and 0.018 for the imaginary part does not remove this feature. Moreover, applying the UT/LMS response function to data measured in the LMS leads to particle volume distributions with a first broad peak and first maximum between 250 and 400 nm diameter (Fig. 10), but also with a second, partly very prominent peak above the Mie resonance. Below about 400 nm the curves for refractive indices with the same real part fall together, as expected. For this representation piece-wise linear fits for the response function were used and the Mie resonance was likewise bridged with a monotonous linear section to have an unambiguous relation between the signal and the particle diameter. This last measure leads to an artificial dip in the volume distributions around 600 nm. However, the second volume peak above 700 nm is outside the Mie resonance and can thus not be explained by this feature. This second maximum is very sensitive to the refractive index and seems to be artificial, in particular for periods of low volcanic influence on the UT/LMS aerosol. As the particles

11611

measured by the CARIBIC OPSS are mostly dry (see Sect. 4.3) the possibility of measuring slightly non-spherical particles was considered, which would lead to a smoother response function (Pinninck et al., 1976; Borrmann et al., 2000). Therefore the UT/LMS response function was calculated again for slightly non-spherical particles with moderate surface structure, described in Pfeifer (2014). The respective new curve is displayed in Fig. 9b. Below 550 nm the non-spherical particle response function does not deviate strongly from the spherical particle response function, but above the Mie resonance level the difference is significant. This new response function is just one realization of many possible non-spherical response functions. However, it is a monotonous function (Fig. 9b) and leads to a smooth particle volume size distribution (Fig. 10), thus solving the problems with the spherical response function above. Hence the non-spherical response function in Fig. 9b was used for the CARIBIC OPSS UT/LMS data evaluation. There can be other reasons, which lead to a similar response function (e.g., unknown properties of the optics or a particle size dependent refractive index); hence the use of a non-spherical particle response function is no proof that the majority of the UT/LMS particles are non-spherical.

## 3.5 OPSS counting efficiency

The counting efficiency of the CARIBIC OPSS, i.e. the ratio of the number of particles the CARIBIC OPSS counts to the number of available particles, is an important correction factor for the post-flight data processing. In the original set-up the laser beam illuminated only half of the air sample, which limited the maximum asymptotic counting efficiency of the original KS-93 to 50 %. Due to the implemented sheath air technique a higher maximum asymptotic counting efficiency could be reached. Using the calibration set-up in Fig. 4 the CARIBIC OPSS counting efficiency was determined for PSL and AS particles with the CPC as reference instrument. Because of existing water peaks, with particle diameters below 100 nm, which would be counted by the CPC but not by the CARIBIC OPSS, only DMA selected particles were used for determining the

11612

OPSS counting efficiency. For our set-up the counting efficiency $\varepsilon(d_p)$ is defined as

$$\varepsilon(d_p) = \frac{N_{OPSS}}{N_{CPC}} \tag{1}$$

with $N$ as the particle number concentration measured at a given particle diameter $d_p$. When using monodisperse PSL particles, the measured particle number concentrations (corrected for the spurious signals at smaller particle diameters, see Sect. 3.2), can be directly compared for each particle size. The four measurement points with PSL standards 125, 200, 350, and 500 nm were complemented with AS particles. These multiply charged AS particles (as result of the DMA) were resolved in size by using 256 channels for the CARIBIC OPSS data analysis. Using these highly resolved data the counting efficiency of the CARIBIC OPSS was calculated iteratively from large particle sizes to smaller ones. For each singlet maximum diameter the number of all multiple charged particles ($N_{multiple}$) measured by the OPSS was summed for all larger size channels $i$ (Eq. 2).

$$N_{multiple} = \sum_i \frac{N_i}{\varepsilon_i} \tag{2}$$

Thereby the counting efficiency for the doublets, triplets and larger particle sizes was taken into account. The respective counting efficiencies were taken from the previous calibration steps. For the first calibration step (largest particles, 500 nm AS), the particle generator was operated with a salt concentration low enough to guarantee that multiply charged particles were not present, hence $N_{multiple}$ was zero.

By subtracting $N_{multiple}$ from the number of particles the CPC counted ($N_{CPC}$), the total number of singly charged particles was calculated ($N_{CPC,s}$; Eq. 3). Dividing the number of singly charged particles the CARIBIC OPSS counted ($N_{OPSS,s}$; Eq. 4, with "a" and "b" the channel borders of the singly charge particle peak) by $N_{CPC,s}$, the OPSS counting efficiency $\varepsilon(d_p)$ at the particle diameter

of the singlets was finally determined (Eq. 5).

$$N_{CPC,s} = N_{CPC} - N_{multiple} \tag{3}$$

$$N_{OPSS,s} = \sum_{i=a}^{b} N_i \tag{4}$$

$$\varepsilon_i = \varepsilon(d_p) = \frac{N_{OPSS,s}}{N_{CPC,s}} \tag{5}$$

The resulting counting efficiency curve is displayed in Fig. 11. Like for the size calibration, all particle diameters were related to an UT aerosol. Above about 200 nm, the OPSS counting efficiency is constant and reaches a maximum asymptotic counting efficiency of 98 %. For smaller particle diameters the counting efficiency decreases. The particle diameter where the counting efficiency is half the maximum asymptotic counting efficiency ($d_{p50}$) characterizes the lower detection limit of a particle counter. Using Eq. (6) as fitting function (Wiedensohler et al., 1997), the CARIBIC OPSS $d_{p50}$ for a mid-latitude UT aerosol was calculated to 152 nm.

$$\varepsilon(d_p) = A - \frac{B}{1 + \exp\left(\frac{d_p - d_{p1}}{d_{p2}}\right)}. \tag{6}$$

## 3.6 OPSS particle coincidence

Although particle coincidence is in general a minor problem for measurements methods using a sheath air technique, the effect of two particles being in the optical field of view at the same time was investigated for the CARIBIC OPSS. For that purpose the number concentrations measured by the CARIBIC OPSS for 200 nm PSL particles and

corrected for the counting efficiency (Sect. 3.5) were compared to the number concentrations measured by the CPC in the calibration set-up (Sect. 3.1). Figure 12 shows the respective results. The coincidence effect is below 3 % for an ambient particle number concentration of 1500 cm$^{-3}$. Considering that, based on CARIBIC measurements, the ambient accumulation mode particle number concentration in the UT/LMS rarely exceeds 100 cm$^3$ (coincidence below 0.2 %) the raw data were not corrected for coincidence in the post-flight data processing.

## 4 Data evaluation

### 4.1 Post-flight data processing

For post-flight analysis of the CARIBIC OPSS data a FORTRAN program was written that converts the raw data into a particle number size distribution. The program first converts the amplified raw signal maxima of a particle pulse to a particle size using the size calibration curve (Sect. 3.4 and Fig. 9). The obtained particle sizes are then sorted into a histogram with logarithmically equidistant size bins. For the current data version (V14), the resolution was set to 10 size channels and 180 s. As the uncertainty of the counting efficiency at particle diameters well below the $d_{p50}$ leads to particle number concentration uncertainties of several tens of percent the CARIBIC particle size distributions do not include data below 140 nm particle diameter. Due to the saturation of the signal amplifiers and in order to be able to clearly resolve at least the maximum of each particle signal the CARIBIC particle size distributions were limited to 1050 nm on the upper end of the size distribution.

To obtain the particle number size distribution, i.e., the number concentration for each size bin, the program calculates the volume flow through the CARIBIC OPSS from the MFC-derived mass flows and the measurement air temperature and pressure. All concentrations are converted from ambient to standard atmospheric conditions ($T$ = 273.15 K, $p$ = 1013.25 hPa). The program also corrects the data for the

11615

counting efficiency of the CARIBIC OPSS (Sect. 3.5) and for particle losses in the inlet and the sampling line between the inlet tip and the CARIBIC OPSS (3 % ± 1 %, Weigelt, 2015). These sampling losses are estimated based on empirical equations from the literature and wind tunnel experiments with another aircraft-borne aerosol inlet (Hermann et al., 2001). Particle coincidence can be neglected for the UT/LMS (see Sect. 3.6). In addition to the particle number size distribution, concentrations of the integral particle number, the particle surface area, the particle volume, the particle mass (assuming a particle density of 1.66 g cm$^{-3}$ based on the same composition used for calculating the refractive index above), as well as the geometric mean particle diameter are calculated. Moreover, the particle surface, volume, and mass distributions can be calculated.

When analyzing the first flight data it was found that high, short-time peaks in the CARIBIC OPSS particle number and mass concentrations correlated well with the occurrence of clouds (Martinsson et al., 2014; Weigelt, 2015). The latter were identified using the cloud water content measured in parallel in situ by the CARIBIC water instruments (Dyroff et al., 2014) and, if this parameter was not available, using the modeled cloud water content from KNMI (www.knmi.nl/samenw/campaign_support/CARIBIC/index.html, last access: 1 July 2015). Following the Kelvin-Köhler theory, the interstitial accumulation mode particle number inside clouds should be lowered due to the activation of these particles to cloud droplets. However, the CARIBIC OPSS particle number size distributions showed for all particle diameters equal or higher particle number concentrations inside clouds compared to outside. Therefore it must be assumed that the CARIBIC OPSS inside cloud measurements are biased by particle artifacts caused by cloud droplet break up at the inlet tip (Korolev et al., 2011, 2013). Consequently, all in-cloud data were flagged as "missing data" in the CARIBIC OPSS data set. These cloud-influenced data fractions amount to 0.6 to 20 % of the OPSS measurements at cruise altitude, depending on the atmospheric region (i.e., LMS or UT).

11616

## 4.2 Comparison with balloon-borne measurements

To evaluate the resulting data we compared the particle number size distributions measured by the CARIBIC OPSS with balloon-borne in situ measurements over Laramie, Wyoming, USA (Deshler et al., 2003). For the comparison periods of low volcanic influence (according to Andersson et al., 2015) in the years 2010 to 2013 were used. The data are considered representative for the background aerosol. Furthermore the data were restricted to the LMS (ozone values between 150–700 ppbv) south of 65° N, as the LMS aerosol shows much less variation with sampling location than the UT aerosol (see Fig. 14). Thus the large spatial distance between Laramie, Wyoming, and the CARIBIC data sampling location has little influence on the comparison. The resulting size distributions are shown in Fig. 13. In order to account for the evaporation of water and thus the shrinking of the aerosol particles during transport through the CARIBIC inlet system (see Sect. 4.3) the CARIBIC size distribution was shifted by 15 % in diameter towards larger particle diameters. Consequently all curves represent ambient distributions. The balloon mean and the CARIBIC OPSS median number size distributions look quite similar in shape and magnitude. However, the balloon number size distribution agrees best with the CARIBIC OPSS 10 % percentile number size distribution, which is about a factor of two lower in concentration than the CARIBIC OPSS median number size distribution. A clear reason for this factor two cannot be given yet, as both instruments are well characterized. The difference in the for the data evaluation used refractive indices, i.e. 1.45-i0.0 (balloon) and 1.47-i0.006 (CARIBIC), cannot account for this factor two as adapting to the balloon data refractive index would shift the CARIBIC particle diameters only by 1–3 %, and this, moreover, mostly towards larger particle diameters. One reason might be that there is still some variability in the LMS aerosol with longitude (both in number and in refractive index) and thus the different sampling locations could contribute to the observed difference. Another reason might be connected to the measurement platform, as one of the two instruments was mounted onboard a jet aircraft whereas the other was ascending on a balloon. A com-

11617

parison between aircraft-borne particle number size distribution measurements given in the literature (de Reus et al., 2000, 2001; Krejci et al., 2003; Schröder et al., 2002; Young et al., 2007; Zaizen et al., 2004) yielded an even much higher scatter between the individual data sets (Weigelt, 2015).

## 4.3 Measurement uncertainties

Concerning the measured particle number size distributions, three kinds of uncertainties have to be considered: the statistical counting uncertainty, the instrumental uncertainty with respect to particle number concentration, and the instrumental uncertainty with respect to particle sizing.

The statistical uncertainty of the particle number concentration measurements arises due to the fact that particle counting follows the Poisson statistics (e.g., Fukutsu et al., 1999; Damit et al., 2014). Consequently the standard deviation $\sigma_N$ due to counting uncertainty of a measured total accumulation mode particle number concentration $N_{140}$ is given by (in percent)

$$\sigma_N = \frac{\sqrt{N_{140}}}{N_{140}} \times 100 = \frac{100}{\sqrt{N_{140}}} \tag{7}$$

The CARIBIC OPSS uncertainty with respect to particle number concentrations is caused by the uncertainties of the OPSS flow rate (14 %), the OPSS counting efficiency (5 % for diameters larger than 200 nm), the particle refractive index (0 % for the total accumulation mode particle number concentration and 15 % for the individual size channels, based on real flight data evaluated with different refractive indices), and the inlet sampling efficiency for accumulation mode particles (estimated to 10 % based on the standard deviation of the wind tunnel experiment particle transmission data of the inlet). To these randomly distributed uncertainties (Gaussian error propagation) the error caused by the spurious particle signals (below 1 %) must be added, whereas coincidence again can be neglected. Error propagation yields a total instru-

11618

mental uncertainty with respect to the particle number concentration of 19 % for the total accumulation mode particle number and 25 % for the individual size channels.

The uncertainty of the CARIBIC OPSS with respect to particle size is determined by three factors: the uncertainty of the size calibration, the use of a single complex refractive index for all aerosols, and the evaporation of particle material during transport through the sampling line. The uncertainty of the size calibration can be estimated, using the width of the Gaussian signal distribution when measuring a monodisperse aerosol. According to laboratory calibrations this uncertainty is 6 % for the CARIBIC OPSS (Weigelt, 2015).

Uncertainties caused by the unknown refractive index of atmospheric particles was estimated for one measurement flight by three refractive indices representative for the mid-latitude upper troposphere, the lowermost stratosphere and the tropical middle troposphere (Weigelt, 2015). For these calculations the ten-hour CARIBIC flight LH317 from Frankfurt/Germany to Johannesburg/South Africa on 15 November 2010 was chosen because it passed all three atmospheric regions. According to this estimate the uncertainty in the OPSS derived particle size is about 15 % in particle diameter, and nearly independent of particle size. This value is derived from the size distributions with the two refractive indices, which yielded the most differing size distribution curves.

Finally, the evaporation of particle material during transport from the inlet system to the CARIBIC OPSS leads to an uncertainty concerning the determined particle size. As the measurement air is heated from about −55 °C in the ambient UT/LMS to about +25 °C in the measurement container, the measured particles can be assumed to be mostly dry. Box model calculations for the evaporation of stratospheric sulfuric acid/water particles in the CARIBIC sampling line indicated that for accumulation mode particles about 84–88 % of the water is evaporated (depending on particle size) when the particles reach the OPSS whereas sulfuric acid almost completely remains particle-bound (1–8 % losses). As the changes in particle size due to the leftover water and the evaporated sulfuric acid partly cancel each other out the measured particle diameter agrees within 5 % with the ambient dry particle diameter. As the real particle

composition in the UT is different from pure sulfuric acid/water (Murphy et al., 2014) and in particular the fraction, composition, and properties of the organic particle material is not known yet it is hard to calculate the respective shrinking of UT particles.

## 5   CARIBIC OPSS application

Since June 2010, the OPSS is part of the CARIBIC measurement container onboard a Lufthansa Airbus A340-600 (www.caribic-atmospheric.com, Brenninkmeijer et al., 2007). In CARIBIC, two to four intercontinental flights per month are carried out with this flying laboratory, as one of the two pillars of IAGOS (In-service Aircraft for a Global Observing System, www.iagos.org). Particle size distributions measured during two of these flights are displayed in Figs. 14 and 15. Figure 14 shows the particle number size distribution for the CARIBIC flight LH454 from Seoul, South Korea to Frankfurt, Germany on 4 December 2013. Almost all cruise altitude data (10.6–12.2 km) were taken in the LMS (see ozone mixing ratio). 86 % of these LMS measurements were in air masses, which are characteristic for air two to three kilometers above the thermal tropopause. As passenger aircraft fly in a narrow cruise altitude range (about 9–12 km), the large distance to the local tropopause can only be reached by the displacement of the local tropopause relative to the aircraft, for instance in a tropopause fold. The particle number size distribution in the LMS shows little variation with sampling region (the time axis in Fig. 14 is virtually a longitude axis, because of the mainly east – west flight track), with a standard deviation of only 9 and 17 % in total accumulation mode particle number and mass concentration, respectively. This variation is moreover mainly caused by changes in the flight altitude, as there are strong vertical gradients in aerosol concentrations in the tropopause region (e.g., Brock et al., 1995; Martinsson et al., 2005).

Figure 15 displays the accumulation mode particle number size distribution for the CARIBIC flight LH319 from Frankfurt, Germany to Bogota, Columbia on 16 November 2010 measured at cruise altitudes of 10.4 to 11.6 km. Three times the aircraft

changed between tropospheric and stratospheric flight sections, which can be clearly seen in the ozone mixing ratio, but also by the aerosol color pattern in Fig. 15. Mid-latitude tropospheric sections show on average a factor of about ten lower accumulation mode particle concentrations (both in number and mass) compared to the stratospheric sections. This concentration difference is caused by the continuous supply of particle mass from the middle and upper stratosphere with the Brewer–Dobson circulation (Deshler, 2008) and the scavenging of accumulation mode particles by clouds in the troposphere (e.g. Ekman et al., 2006).

## 6 Conclusions

A new Optical Particle Size Spectrometer (OPSS) for aircraft-borne measurements of the particle number size distribution in the upper troposphere and lowermost stratosphere between 130 and 1110 nm diameter is presented in this study. The core instrument, a commercial RION KS-93 particle sensor, was modified to record individual particle pulse signals and thus to adapt sampling time resolution and particle size bin width at any time after measurement. Because of the robust synthetic quartz optics the particle signals show no pressure dependency in the operating pressure range of 200 to 1000 hPa. Installed into a 19″ EMC rack unit the modified KS-93 together with a data acquisition and a new airflow system composes the new OPSS. The particle counting efficiency of the OPSS could be increased from originally 50 to 98 % by using a sheath air technique, as shown by polystyrene latex and ammonium sulfate particle calibration measurements. The sheath air reduced the probability of particle coincidence to less than 3 % for an ambient particle number concentration of 1500 cm$^{-3}$. The occurrence of spurious particle pulses was suppressed below 1 % due to the sheath air and the application of an inter-arrival time filter on the data. The latter, however, works only for low ambient particle number concentrations of about 200 cm$^{-3}$ or less in the accumulation mode, as for instance encountered in the free troposphere and lowermost stratosphere. The size response function of the OPSS, which connects the measured

11621

scattered light signal to the particle diameter, was derived from polystyrene latex calibration measurements and model calculations for spherical and slightly non-spherical particles. The non-spherical particle response function was finally chosen for data evaluation, as it leads to a smoother particle volume distribution curve. A comparison with LMS particle number size distributions measured from balloons (Deshler et al., 2003) yielded an agreement within a factor of two in number concentration.

Since June 2010 the new OPSS is regularly flown once per month for four intercontinental flights inside the CARIBIC (Civil Aircraft for Regular Investigation of the Atmosphere Based on an Instrument Container) measurement container onboard a Lufthansa Airbus (Brenninkmeijer et al., 2007). Since then, the CARIBIC OPSS has measured accumulation mode particle number size distributions on more than one million flight kilometers, mainly in the northern hemispheric UT/LMS (see www.caribic-atmospheric.com/2005/Flight_Scheduling.html last access: 1 July 2015). Besides information about UT/LMS aerosol particle transport, transformation, lifetime and trends, these measurements provide a unique data set for the validation of remote sensing instruments or global atmospheric aerosol models.

## References

Andersson, S. M., Martinsson, B. G., Vernier, J. P., Friberg, J., Brenninkmeijer, C. A. M., Hermann, M., van Velthoven, P. F. J., and Zahn, A.: Significant radiative impact of volcanic
11622

aerosol in the lowermost stratosphere, Nat. Commun., 6, 7692, doi:10.1038/ncomms8692, 2015.

Bohren, C. F. and Huffman, D. R.: Absorption and Scattering of Light by Small Particles, John Wiley & Sons, New York, 530 pp., 1983.

Borrmann, S., Luo, B., and Mishchenko, M.: Application of the T-Matrix method to the measurement of aspherical (ellipsoidal) particles with forward scattering optical particle counters, J. Aerosol Sci., 31, 789–799, 2000.

Brenninkmeijer, C. A. M., Crutzen, P., Boumard, F., Dauer, T., Dix, B., Ebinghaus, R., Filippi, D., Fischer, H., Franke, H., Frieß, U., Heintzenberg, J., Helleis, F., Hermann, M., Kock, H. H., Koeppel, C., Lelieveld, J., Leuenberger, M., Martinsson, B. G., Miemczyk, S., Moret, H. P., Nguyen, H. N., Nyfeler, P., Oram, D., O'Sullivan, D., Penkett, S., Platt, U., Pupek, M., Ramonet, M., Randa, B., Reichelt, M., Rhee, T. S., Rohwer, J., Rosenfeld, K., Scharffe, D., Schlager, H., Schumann, U., Slemr, F., Sprung, D., Stock, P., Thaler, R., Valentino, F., van Velthoven, P., Waibel, A., Wandel, A., Waschitschek, K., Wiedensohler, A., Xueref-Remy, I., Zahn, A., Zech, U., and Ziereis, H.: Civil Aircraft for the regular investigation of the atmosphere based on an instrumented container: The new CARIBIC system, Atmos. Chem. Phys., 7, 4953–4976, doi:10.5194/acp-7-4953-2007, 2007.

Brock, C. A., Hamill, P., Wilson, J. C., Jonsson, H. H., and Chan, K. R.: Particle formation in the upper tropical troposphere: a source of nuclei for the stratospheric aerosol, Science, 270, 1650–1653, 1995.

Cai, Y., Snider, J. R., and Wechsler, P.: Calibration of the passive cavity aerosol spectrometer probe for airborne determination of the size distribution, Atmos. Meas. Tech., 6, 2349–2358, doi:10.5194/amt-6-2349-2013, 2013.

Charlson, R. J., Schwartz, S. E., Hales, J. M., Cess, R. D., Coakley Jr., J. A., Hansen, J. E., and Hofmann, D. J.: Climate forcing by anthropogenic aerosols, Science, 255, 423–430, doi:10.1126/science.255.5043.423, 1992.

Damit, B., Wu, C.-Y., and Cheng, M.-D.: On the validity of the poisson assumption in sampling nanometer-sized aerosols, Aerosol Sci. Tech., 48, 562–570, doi:10.1080/02786826.2014.899682, 2014.

de Reus, M., Ström, J., Curtius, J., Pirjola, Vignati, E., Arnold, F., Hansson, H. C., Kulmala, M., Lelivield, J., and Raes, F.: Aerosol production and growth in the upper free troposphere, J. Geophys. Res., 105, 24751–24762, 2000.

11623

de Reus, M., Krejci, R., Williams, J., Fischer, H., Scheele and Ström, R.: Vertical and horizontal distributions of the aerosol number concentration and size distribution over the northern Indian Ocean, J. Geophys. Res., 106, 28629–28641, doi:10.1029/2001JD900017, 2001.

Deshler, T.: A review of global stratospheric aerosol: measurements, importance, life cycle, and local stratospheric aerosol, Atmos. Res., 90, 223–232, 2008.

Deshler, T., Hervig, M. E., Hofmann, D. J., Rosen, J. M., and Liley, J.: Thirty years of in situ stratospheric aerosol size distribution measurements from Laramie, Wyoming (41° N), using balloon-borne instruments, J. Geophys. Res., 108, 4167, doi:10.1029/2002JD002514, 2003.

Dyroff, C., Zahn, A., Christner, E., Forbes, R., Tompkins, A. M., and van Velthoven, P. F. J.: Comparison of ECMWF analysis and forecast humidity data to CARIBIC upper troposphere and lower stratosphere observations, Q. J. Roy. Meteor. Soc., 141, 833–844, doi:10.1002/qj.2400, 2014.

Ekman, A. M. L., Wang, C., Ström, J., and Krejci, R.: Explicit simulation of aerosol physics in a cloud-resolving model: aerosol transport and processing in the free troposphere, J. Atmos. Sci., 63, 682–696, 2006.

Fukutsu, K., Yamada, Y., Koizumi, A., and Shimo, M.: A statistical study on the design of particle count measurements, J. Aerosol Res. Jpn., 4, 55–62, 1999.

Gebhart, J.: Optical direct-reading techniques: light intensity systems, in: Aerosol Measurement: Principles, Techniques, and Applications, edited by: Baron, P. A. and Willeke, K., Wiley-Interscience, New York, USA, 419–454, 2001.

Hermann, M. and Wiedensohler, A.: Counting efficiency of condensation particle counters at low-pressures with illustrative data from the upper troposphere, J. Aerosol Sci., 32, 975–991, 2001.

Hermann, M., Stratmann, F., Wilck, M., and Wiedensohler, A.: Sampling characteristics of an aircraft-borne aerosol inlet system, J. Atmos. Ocean. Tech., 18, 7–19, 2001.

Korolev, A. V., Emery, E. E., Strapp, J. W., Cober, S. G., Isaac, G. A., Wasey, M., and Marcotte, D.: Small ice particles in tropospheric clouds: fact or artifact?, B. Am. Meteorol. Soc., 91, 967–973, doi:10.1175/2010BAMS3141.1, 2011.

Korolev, A. V., Emery, E. F., Strapp, J. W., Cober, S. G., and Isaac, G. A.: Quantification of the effects of shattering on airborne ice particle measurements, J. Atm. Ocean. Tech., 30, 2527–2553, doi:10.1175/JTECH-D-13-00115.1, 2013.

Krejci, R., Ström, J., de Reus, M., Hoor, P., Williams, J., Fischer, H., and Hansson, H.-C.: Evolution of aerosol properties over the rain forest in Surinam, South America, ob-

11624

served from aircraft during the LBA-CLAIRE 98 experiment, J. Geophys. Res., 108, 4561, doi:10.1029/2001JD001375, 2003.

Mann, G. W., Carslaw, K. S., Reddington, C. L., Pringle, K. J., Schulz, M., Asmi, A., Spracklen, D. V., Ridley, D. A., Woodhouse, M. T., Lee, L. A., Zhang, K., Ghan, S. J., Easter, R. C., Liu, X., Stier, P., Lee, Y. H., Adams, P. J., Tost, H., Lelieveld, J., Bauer, S. E., Tsigaridis, K., van Noije, T. P. C., Strunk, A., Vignati, E., Bellouin, N., Dalvi, M., Johnson, C. E., Bergman, T., Kokkola, H., von Salzen, K., Yu, F., Luo, G., Petzold, A., Heintzenberg, J., Clarke, A., Ogren, J. A., Gras, J., Baltensperger, U., Kaminski, U., Jennings, S. G., O'Dowd, C. D., Harrison, R. M., Beddows, D. C. S., Kulmala, M., Viisanen, Y., Ulevicius, V., Mihalopoulos, N., Zdimal, V., Fiebig, M., Hansson, H.-C., Swietlicki, E., and Henzing, J. S.: Intercomparison and evaluation of global aerosol microphysical properties among AeroCom models of a range of complexity, Atmos. Chem. Phys., 14, 4679–4713, doi:10.5194/acp-14-4679-2014, 2014.

Martinsson, B. G., Nguyen, H. N., Brenninkmeijer, C. A. M., Zahn, A., Heintzenberg, J., Hermann, M., and van Velthoven, P. F. J.: Characteristics and origin of lowermost stratospheric aerosol at northern midlatitudes under volcanically quiescent conditions based on CARIBIC observations, J. Geophys. Res., 110, D12201, doi:10.1029/2004JD005644, 2005.

Martinsson, B. G., Friberg, J., Andersson, S. M., Weigelt, A., Hermann, M., Assmann, D., Voigtländer, J., Brenninkmeijer, C. A. M., van Velthoven, P. J. F., and Zahn, A.: Comparison between CARIBIC Aerosol Samples Analysed by Accelerator-Based Methods and Optical Particle Counter Measurements, Atmos. Meas. Tech., 7, 2581–2596, doi:10.5194/amt-7-2581-2014, 2014.

Murphy, D. M., Froyd, K. D., Schwarz, J. P., and Wilson, J. C.: Observations of the chemical composition of stratospheric aerosol particles, Q. J. Roy. Meteor. Soc., 140, 1269–1278, doi:10.1002/qj.2213, 2014.

Nguyen, H. N., Gudmundsson, A., and Martinsson, B. G.: Design and calibration of a multichannel aerosol sampler for studies of the tropopause region from the CARIBIC platform, Aerosol Sci. Tech., 40, 649–655, 2006.

Pfeifer, S.: Verknüpfung aerodynamischer und optischer Eigenschaften nichtkugelförmiger atmosphärischer Grobstaubpartikel, PhD Thesis, University Leipzig, Dresden, Germany, available at: http://www.qucosa.de/recherche/frontdoor/cache.off?tx_slubopus4frontend[id]=15856 (last access: 3 November 2015), 2014.

11625

Pinnick, R. G., Carroll, D. E., and Hoffmann, D. J.: Polarized light scattered from monodisperse randomly oriented nonspherical aerosol particles: measurements, Appl. Optics, 15, 384–393, 1976.

Rauthe-Schöch, A., Weigelt, A., Hermann, M., Martinsson, B. G., Baker, A. K., Heue, K.-P., Brenninkmeijer, C. A. M., Zahn, A., Scharffe, D., Eckhardt, S., Stohl, A., and van Velthoven, P. F. J.: CARIBIC aircraft measurements of Eyjafjallajökull volcanic clouds in April/May 2010, Atmos. Chem. Phys., 12, 879–902, doi:10.5194/acp-12-879-2012, 2012.

Rosenberg, P. D., Dean, A. R., Williams, P. I., Dorsey, J. R., Minikin, A., Pickering, M. A., and Petzold, A.: Particle sizing calibration with refractive index correction for light scattering optical particle counters and impacts upon PCASP and CDP data collected during the Fennec campaign, Atmos. Meas. Tech., 5, 1147–1163, doi:10.5194/amt-5-1147-2012, 2012.

Schröder, F., Kärcher, B., Fiebig, M., and Petzold, A.: Aerosol states in the free troposphere at northern midlatitudes, J. Geophys. Res., 107, 8126, doi:10.1029/2000JD000194, 2002.

Seinfeld, J. H. and Pandis, S. N.: Atmospheric Chemistry and Physics: from Air Pollution to Climate Change, 1st edn, J. Wiley, New York, USA, 1326 pp., 1998.

Weigelt, A.: An optical particle counter for the regular application onboard a passenger aircraft: instrument modification, characterization and results from the first year of operation, Ph.D. thesis, Universität Leipzig, Leipzig, 204 pp., 2015.

Wiedensohler, A., Orsini, D., Covert, D. S., Coffmann, D., Cantrell, W., Havlicek, M., Brechtel, F. J., Russell, L. M., Weber, R. J., Gras, J., Hudson, J. G., and Litchy, M.: Intercomparison study of size-dependent counting efficiency of 26 condensation particle counters, Aerosol Sci. Tech., 27, 224–242, 1997.

Wiedensohler, A., Birmili, W., Nowak, A., Sonntag, A., Weinhold, K., Merkel, M., Wehner, B., Tuch, T., Pfeifer, S., Fiebig, M., Fjäraa, A. M., Asmi, E., Sellegri, K., Depuy, R., Venzac, H., Villani, P., Laj, P., Aalto, P., Ogren, J. A., Swietlicki, E., Williams, P., Roldin, P., Quincey, P., Hüglin, C., Fierz-Schmidhauser, R., Gysel, M., Weingartner, E., Riccobono, F., Santos, S., Grüning, C., Faloon, K., Beddows, D., Harrison, R., Monahan, C., Jennings, S. G., O'Dowd, C. D., Marinoni, A., Horn, H.-G., Keck, L., Jiang, J., Scheckman, J., McMurry, P. H., Deng, Z., Zhao, C. S., Moerman, M., Henzing, B., de Leeuw, G., Löschau, G., and Bastian, S.: Mobility particle size spectrometers: harmonization of technical standards and data structure to facilitate high quality long-term observations of atmospheric particle number size distributions, Atmos. Meas. Tech., 5, 657–685, doi:10.5194/amt-5-657-2012, 2012.

11626

Winker, D. M., Tackett, J. L., Getzewich, B. J., Liu, Z., Vaughan, M. A., and Rogers, R. R.: The global 3-D distribution of tropospheric aerosols as characterized by CALIOP, Atmos. Chem. Phys., 13, 3345–3361, doi:10.5194/acp-13-3345-2013, 2013.

Young, L.-H., Benson, D. R., Montanaro, W. M., Lee, S.-H., Pan, L. L., Rogers, D. C., Jensen, J., Stith, J. L., Davis, C. A., Campos, T. L., Bowman, K. P., Cooper, W. A., and Lait, L. R.: Enhanced new particle formation observed in the northern midlatitude tropopause region, J. Geophys. Res., 112, D10218, doi:10.1029/2006JD008109, 2007.

Zaizen, Y., Okada, K., Ikegami, M., Sawa, Y., and Makino, Y.: Number-size distributions of aerosol particles in the free troposphere over the Northwestern Pacific Ocean – influence of Asian outflow and tropical air transport, J. Meteorol. Soc. Jpn., 82, 1147–1160, 2004.

**Figure 1.** RION KS-93 particle sensor (www.rion.co.jp/english/product/particle/assets/KS-93-E.pdf, last access: 1 July 2015).
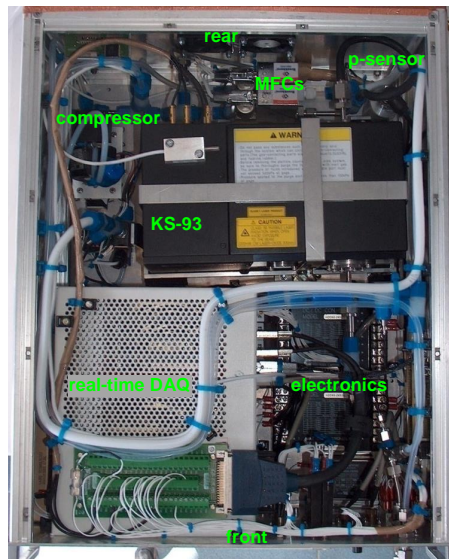
**Figure 2.** Top view of the CARIBIC Optical Particle Size Spectrometer (OPSS).
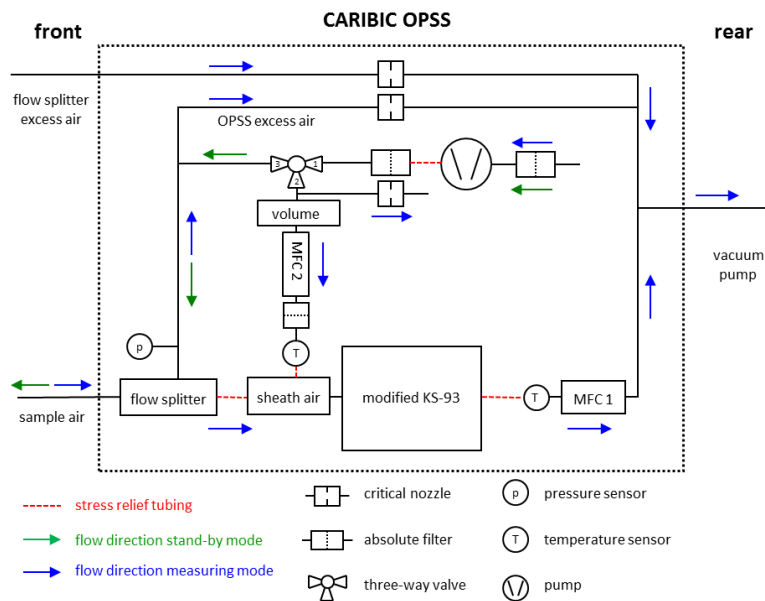
**Figure 3.** Air flow diagram of the CARIBIC OPSS.
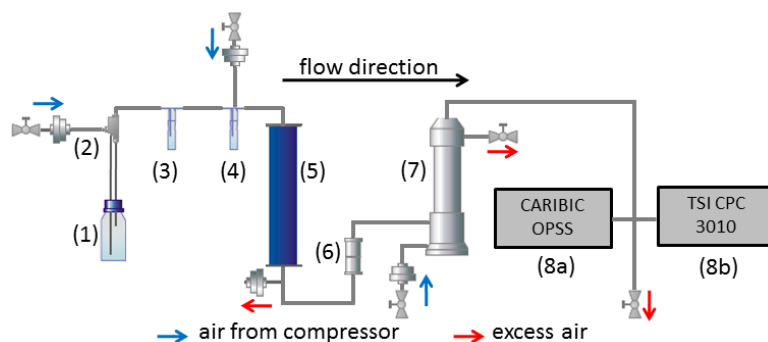
**Figure 4.** OPSS calibration setup with (1) glass bottle containing the particle material in aqueous solution or suspension, (2) particle generator (nebulizer), (3) droplet trap, (4) dilution unit, (5) silica gel drier, (6) bipolar diffusion charger, and (7) Differential Mobility Analyzer (DMA). A TSI Condensation Particle Counter (CPC 3010) was operated in parallel to the CARIBIC OPSS (8a and 8b) as reference for the counting efficiency measurements.
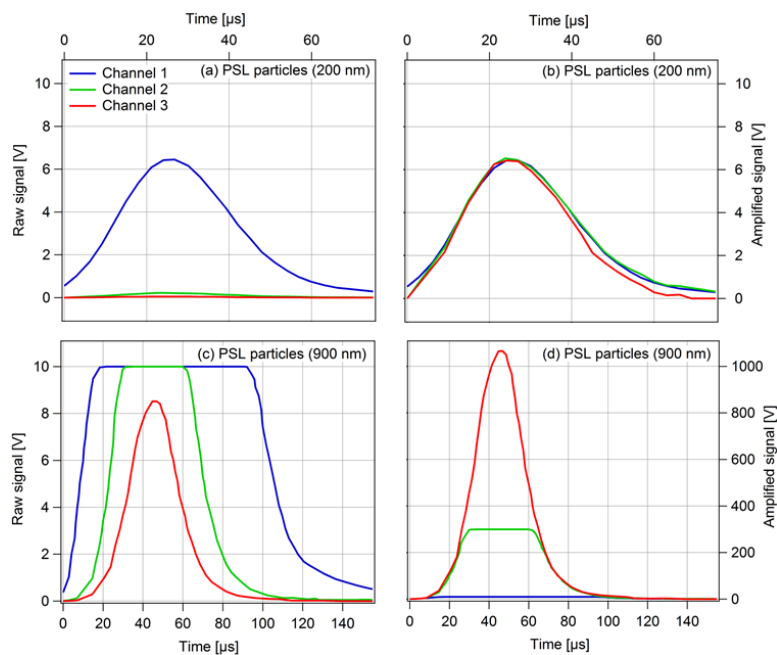
**Figure 5.** Particle signal pulses measured with all three CARIBIC OPSS channels for 200 and 900 nm diameter polystyrene latex (PSL) particles. Figure **(a)** and **(c)** show the raw signals at the SMB connectors of the modified KS-93. The amplified signals (factor of 30 for Ch2 and 125 for Ch3), used for data analysis, are shown in **(b)** and **(d)**, respectively.
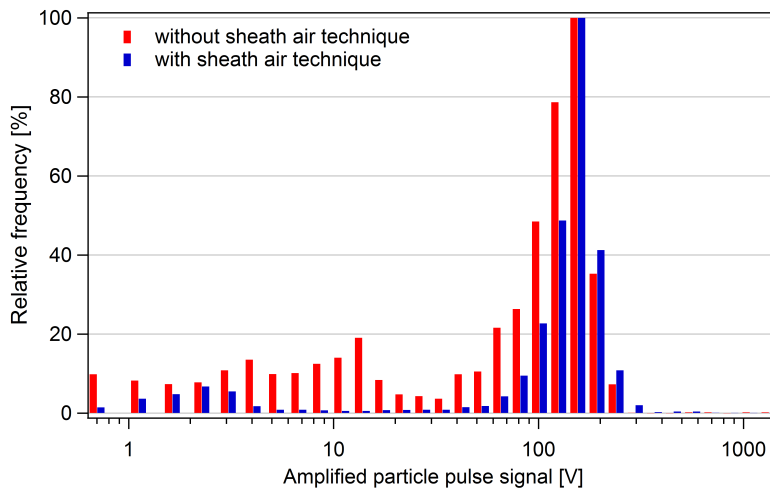
**Figure 6.** Signal intensity distribution measured with the CARIBIC OPSS for 350 nm PSL particles without and with implemented sheath air technique.
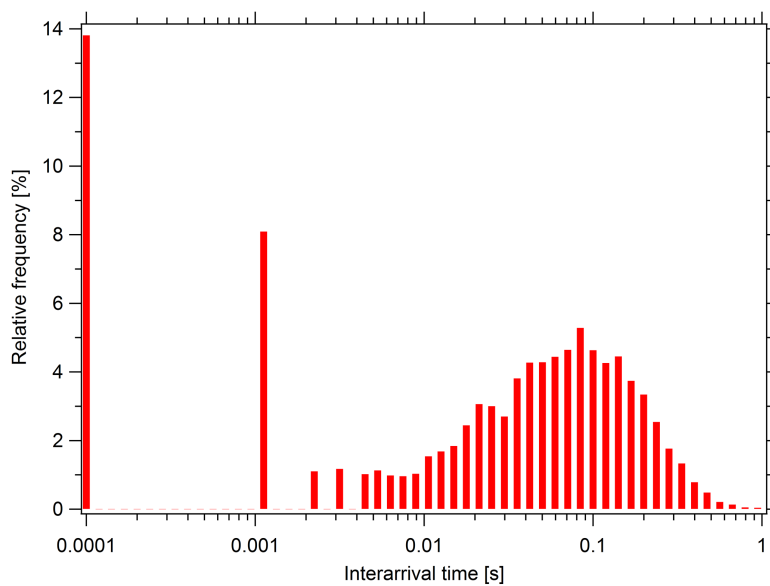
**Figure 7.** Inter-arrival time histogram of the CARIBIC OPSS for 500 nm PSL particles and a number concentration of about 60 particles per cubic centimeter.
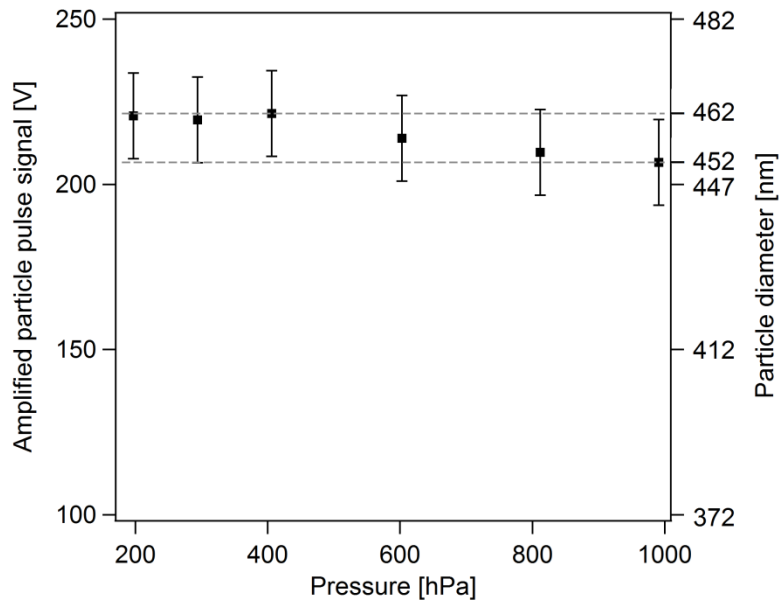
**Figure 8.** Particle signal pressure dependency of the CARIBIC OPSS for 450 nm PSL particles. Error bars indicate plus/minus one size channel uncertainty (out of 230 in total) in the determination of the peak distribution maximum.

11635
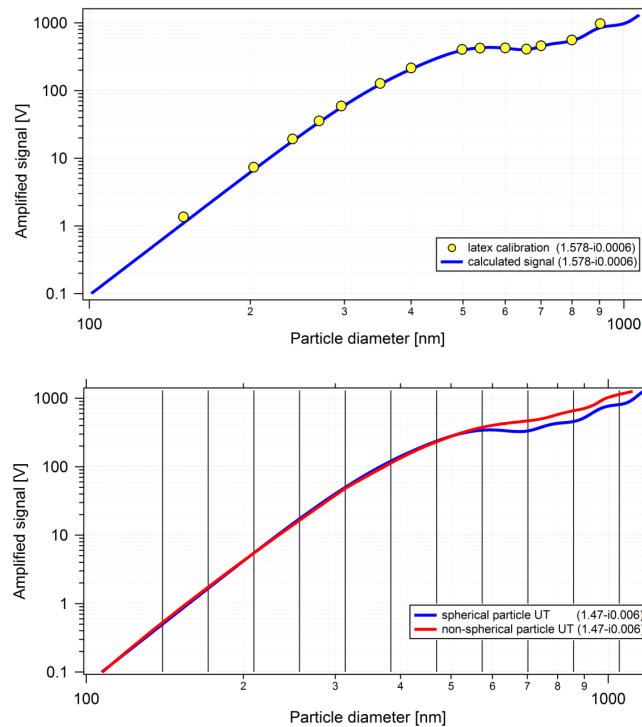
**Figure 9.** Response function of the CARIBIC OPSS for perpendicular polarized light: upper panel: PSL calibration measurement data and calculated PSL response function, lower panel: calculated response functions for spherical and slightly non-spherical UT particles. Solid vertical lines indicate the finally chosen particle size channel borders.

11636
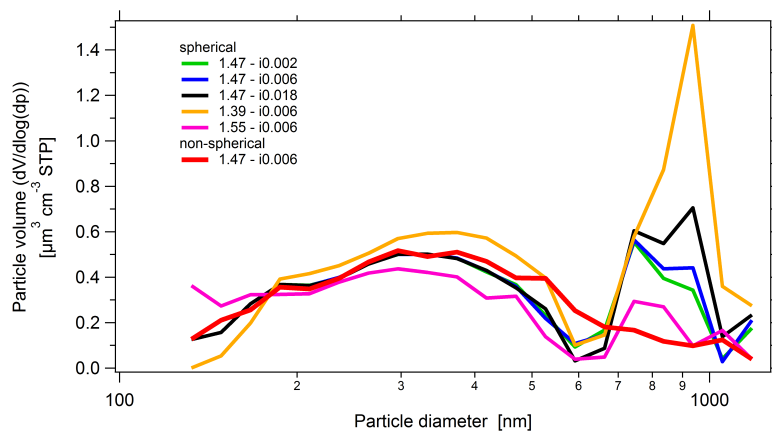
**Figure 10.** Particle volume distribution measured in the LMS during the CARIBIC flight LH339 on 19 April 2011 from Frankfurt, Germany to Vancouver, Canada. Same data are displayed for six different refractive indices and using six different OPSS response functions.
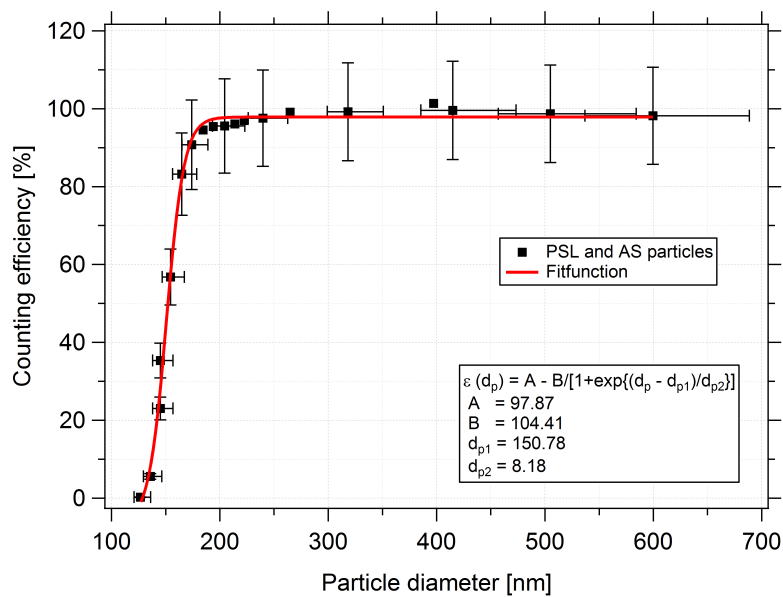
**Figure 11.** Counting efficiency of the CARIBIC OPSS for UT particles (refractive index of 1.47-i0.006).

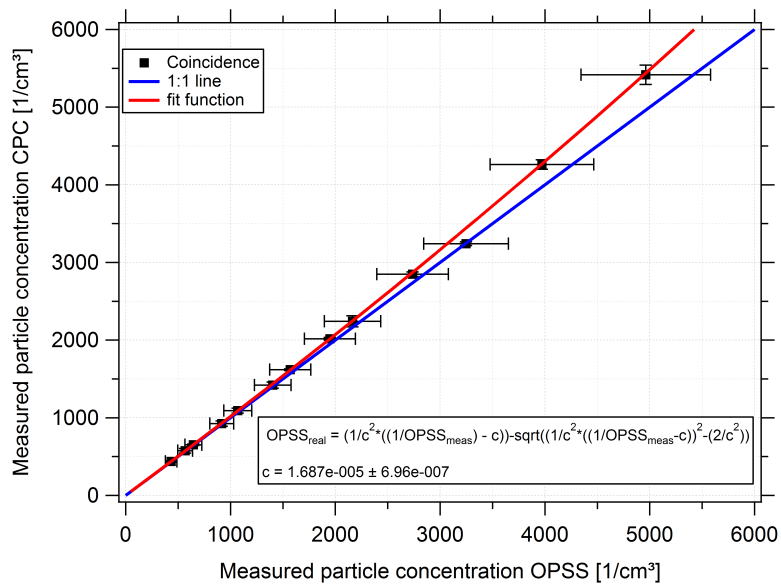$$OPSS_{real} = (1/c^2 \ast ((1/OPSS_{meas}) - c)) - sqrt((1/c^2 \ast ((1/OPSS_{meas} - c))^2 - (2/c^2)))$$

$$c = 1.687e\text{-}005 \pm 6.96e\text{-}007$$

**Figure 12.** Particle coincidence in the CARIBIC OPSS measured for 200 nm PSL particles.
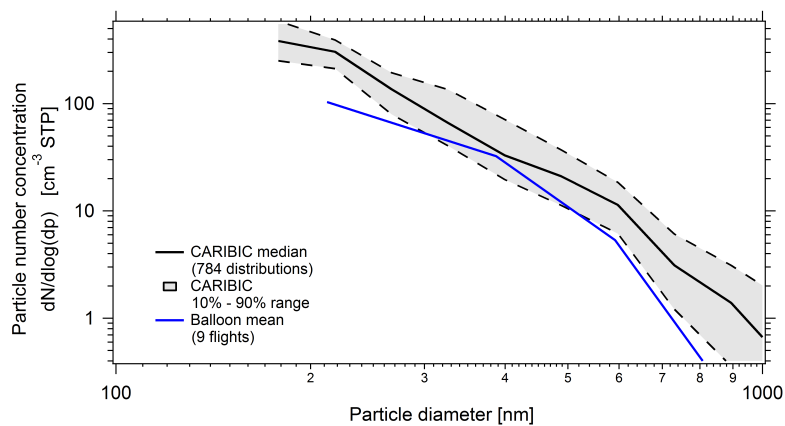
**Figure 13.** Comparison of particle number size distributions measured with a balloon-borne OPSS (Deshler et al.,2003) and the CARIBIC OPSS. Underlying data were all taken in the mid-latitude LMS (south of 65° N, 150–700 ppbv ozone) from periods in 2010–2013 with little or no volcanic influence on the LMS aerosol (see Andersson et al., 2015; Fig. 1).
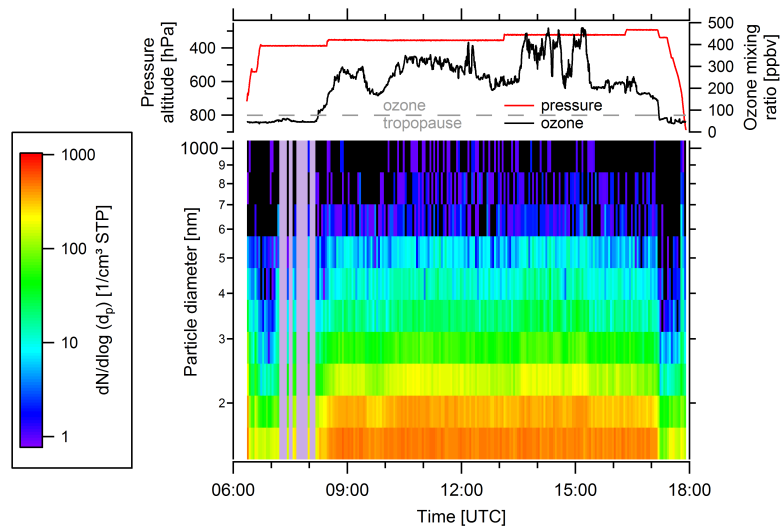
**Figure 14.** Accumulation mode particle number size distribution for the CARIBIC flight LH454 from Seoul, South Korea to Frankfurt, Germany on 4 December 2013. Cruise level data are obtained almost exclusively in the LMS, in air masses which are characteristic for air from two to three kilometers above the thermal tropopause (see www.knmi.nl/samenw/campaign_support/CARIBIC/041213a/index.html, last access: 1 July 2015). The red line gives the aircraft pressure altitude, the black line the ozone mixing ratio and the color code the particle number concentration in 10 particle size bins. Grey bars indicate periods of inside cloud measurements.
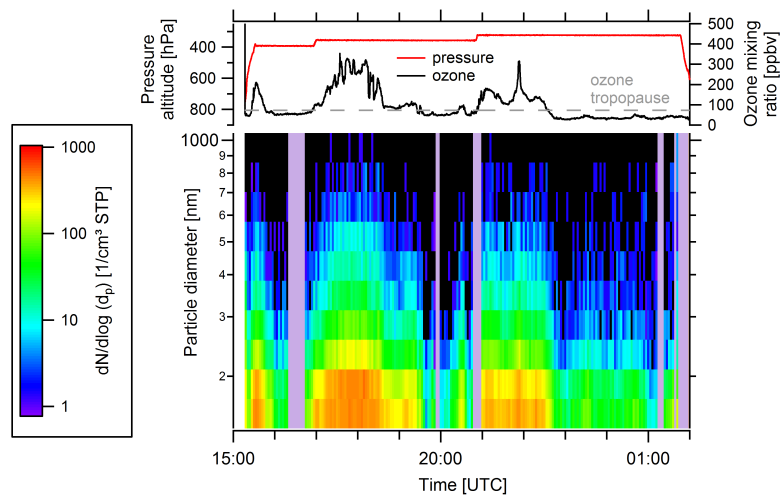
**Figure 15.** Accumulation mode particle number size distribution for the CARIBIC flight LH319 from Frankfurt, Germany to Bogota, Columbia on 16 November 2010. This flight is characterized by alternating tropospheric and stratospheric flight sections (see ozone mixing ratio and www.knmi.nl/samenw/campaign_support/CARIBIC/161110/index.html, last access: 1 July 2015). Same representation as in Fig. 14.